

Non-Linear Optical Microscopy Sheds Light on Cardiovascular Disease

Valentina Caorsi^{1*}, Christopher Toepfer¹, Markus B. Sikkell², Alexander R. Lyon^{2,3}, Ken MacLeod³, Mike A. Ferenczi^{1,4}

1 Molecular Medicine, National Heart and Lung Institute, Imperial College London, London, United Kingdom, **2** Myocardial Function, National Heart and Lung Institute, Imperial College London, London, United Kingdom, **3** Cardiovascular Biomedical Research Unit, Royal Brompton Hospital, London, United Kingdom, **4** Lee Kong Chian School of Medicine, Nanyang Technological University, Singapore, Singapore

Abstract

Many cardiac diseases have been associated with increased fibrosis and changes in the organization of fibrillar collagen. The degree of fibrosis is routinely analyzed with invasive histological and immunohistochemical methods, giving a limited and qualitative understanding of the tissue's morphological adaptation to disease. Our aim is to quantitatively evaluate the increase in fibrosis by three-dimensional imaging of the collagen network in the myocardium using the non-linear optical microscopy techniques Two-Photon Excitation microscopy (TPE) and Second Harmonic signal Generation (SHG). No sample staining is needed because numerous endogenous fluorophores are excited by a two-photon mechanism and highly non-centrosymmetric structures such as collagen generate strong second harmonic signals. We propose for the first time a 3D quantitative analysis to carefully evaluate the increased fibrosis in tissue from a rat model of heart failure post myocardial infarction. We show how to measure changes in fibrosis from the backward SHG (B_{SHG}) alone, as only backward-propagating SHG is accessible for true *in vivo* applications. A 5-fold increase in collagen I fibrosis is detected in the remote surviving myocardium measured 20 weeks after infarction. The spatial distribution is also shown to change markedly, providing insight into the morphology of disease progression.

Citation: Caorsi V, Toepfer C, Sikkell MB, Lyon AR, MacLeod K, et al. (2013) Non-Linear Optical Microscopy Sheds Light on Cardiovascular Disease. PLoS ONE 8(2): e56136. doi:10.1371/journal.pone.0056136

Editor: Alena Talkachova, University of Minnesota, United States of America

Received: August 9, 2012; **Accepted:** January 5, 2013; **Published:** February 7, 2013

Copyright: © 2013 Caorsi et al. This is an open-access article distributed under the terms of the Creative Commons Attribution License, which permits unrestricted use, distribution, and reproduction in any medium, provided the original author and source are credited.

Funding: This work was supported by the Royal Society (Newton International fellowship to VC), the Biotechnology and Biological Sciences Research Council [grant number BB/1019448/1] and the Wellcome Trust [grant numbers 091460/Z/10/Z, 092852/Z/10/Z]. ARL was supported by a British Heart Foundation Intermediate Research Fellowship (FS/11/67/28954) and the National Institute for Health Research-funded Cardiovascular Biomedical Research Unit at the Royal Brompton Hospital. The funders had no role in study design, data collection and analysis, decision to publish, or preparation of the manuscript.

Competing Interests: The authors have declared that no competing interests exist.

* E-mail: v.caorsi@imperial.ac.uk

Introduction

The importance of increased fibrosis in heart pathology and dysfunction has been increasingly noted in diseases including dilated, ischaemic and hypertrophic cardiomyopathies. In healthy tissue the extracellular fibrillar collagen forms a dynamic scaffold with important functions for tissue integrity and efficiency of systolic contraction and diastolic relaxation [1]. Increased collagen deposition in reactive fibrosis leads to altered myocardial function, specifically reducing tissue compliance and impairing both contraction and relaxation [2]. The degree of fibrosis is routinely analyzed in experimental models, and at *post mortem* in human hearts, with histological and immunohistochemical methods. These require invasive extraction of tissue samples, thin slicing by microtomes (1–10 μm sections), embedding, fixation, and staining procedure [3,4]. Although these methods allow collagen to be clearly distinguished, they report from a thin layer of the sample under investigation, giving a limited and qualitative understanding of the tissue's morphological adaptation to disease. Furthermore myocardial tissue acquisition in the clinic is limited, and sample processing can introduce artifacts thus limiting its use [5]. Three-dimensional imaging of the collagen network in the myocardium is required to quantitatively assess the status of fibrosis *in vivo* and hence understand how changes in its production

affect the progression of cardiac dysfunction. Recently non-linear optical microscopy has been shown to be a powerful tool for non-invasive imaging of thick specimens [6,7]. In particular two-photon excitation (TPE) and second harmonic generation (SHG), arising from the non linear interaction of intense coherent optical radiation with matter, have been cleverly exploited to obtain information otherwise inaccessible by conventional microscopy [8]. TPE fluorescence and SHG are particularly suitable for imaging thick samples as both processes intrinsically give optical sectioning capability. Furthermore the infrared excitation light used to induce the two-photon excitation process can enter deeper into the sample because scattering is reduced [9,10]. There is no need for sample staining, thus removing major sources of artifact: SHG arises from a particular type of molecule lacking a center of symmetry (as collagen, microtubules, myosin) and numerous endogenous fluorophores can be excited by a two-photon mechanism [11–14]. Collagen is particularly suitable for SHG collection as the inherent chirality of the helices increases the overall asymmetry thus increasing the second order response. In particular collagen type I and II have been shown to experimentally produce sufficient SHG signals, while collagen type III has a much weaker response [6]. The combination of these two techniques has already provided a new tool for diagnosis of many diseases characterized by defects or changes in the assembly of

collagen in a variety of tissues [15,16,17]. However, to our knowledge, only qualitative or semi-quantitative analysis has been performed in cardiac disease [18,19,20].

Our aim is to combine the use of TPE (to visualize endogenous fluorophores like elastin and myocyte proteins) with the simultaneous collection of SHG from collagen fibrils (type I) in thick cardiac tissues to quantitatively evaluate the increase in fibrosis by analyzing the backward SHG (B_{SHG}) alone, as only backward-propagating SHG is accessible for future *in vivo* applications. In particular we propose a 3D intensity-based and volumetric method which can be easily implemented in any laser scanning microscope equipped with multiphoton excitation with no modifications to the light path, thus enabling and enhancing its applicability. To validate the proposed methodology we evaluate collagen presence in the non-infarcted, viable portion of the left ventricle in a rat model of myocardial infarction [21]. In this model the anterior wall becomes scarred and clearly contains substantial collagen. The remodeling process that occurs in the remainder of the left ventricular wall includes interstitial collagen deposition in non-infarcted tissue, contributing to the decline in the function of this surviving muscle [22,23,24]. We demonstrate a 5-fold increase in collagen fibrosis 20 weeks after infarction. The spatial distribution within the observed volume also changes markedly, providing insight into the morphology of disease progression. The results obtained show how a quantitative evaluation of fibrillar collagen in fresh, untreated tissues is possible, giving information otherwise inaccessible with routine histology methods, thus shedding light on myocardium morphological adaptations to disease *in vivo*.

Materials and Methods

Animal model for heart failure

All animal surgical procedures and perioperative management were carried out in accordance with the United Kingdom Home Office Animals (Scientific Procedures) Act 1986, which conforms to the Guide for the Care and Use of Laboratory Animals published by the US National Institutes of Health under assurance number A5634-01 (NIH publication No. 85-23, revised 1996). The protocol was approved by the Imperial College Ethical Review Committee (PPL: 70/6568 and 70/7399). Adult male Sprague-Dawley rats (250–300 g) underwent proximal left anterior descending coronary artery ligation to induce chronic myocardial infarction [21]. Anaesthesia was induced by administration of 5% isoflurane for induction reducing to 2% isoflurane once intubated and ventilated. It was ensured that pain reflexes were absent prior to an incision being made. Pre-operatively, buprenorphine was administered subcutaneously at a dose of 0.05 mg/kg to ensure adequate analgesia in addition to anaesthesia. Further doses of buprenorphine were administered as required post-operatively if there was any sign of distress. Additionally enrofloxacin (5 mg/kg) and 0.9% saline (10 ml/kg) were administered pre-operatively. Rats were sacrificed by cervical dislocation following brief exposure to 5% isoflurane until righting reflex was lost. Age matched rats which had not undergone surgery were used as controls. Animals were sacrificed at 20 weeks post-surgical intervention by which time a severe heart-failure phenotype has developed. Rapid explantation of rat hearts was performed and hearts were immediately massaged in a modified oxygenated and iced Krebs-Henseleit (KH) solution (composition in mM: 119 NaCl, 4.7 KCl, 0.94 MgSO₄, 1 CaCl₂, 1.2 KH₂PO₄, 25 NaHCO₃, 11.5 glucose) containing 40 mM BDM and Heparin. Hearts were cannulated through the aorta for retrograde perfusion by Langendorff apparatus with oxygenated KH solution [25]. Trabecular preparations (100–120 μm in diameter and

1–2 mm in length) were excised from the inner wall of the left ventricle, T-clipped and permeabilised in a Relaxing solution (composition in mM: 100 TES, 7.8 MgCl₂, 5.7 Na₂ATP, 25 EGTA, 21.2 Na₂CP, 20 GLH, pH 7.1 at 20°C and ionic strength 200 mM) containing 2% Triton for 30 minutes, and stored at –20°C overnight in a relaxing solution containing 50% glycerol for use the following day. All the measurements were performed in relaxing solution which mimics the relaxed state in muscle and tissues with 0Ca and high ATP (zero calcium ensures no activation and high ATP ensures no rigor contractions). The effect of relaxing solution on the B_{SHG} intensity is addressed in the section *Maximizing Backward Collection* where a comparison with solutions at different NaCl concentrations is carried out.

Histology staining

For histological analysis, left ventricular tissues were washed in sterile phosphate-buffered saline, fixed in 4% paraformaldehyde, processed for paraffin embedding. 4 μm thick sections were stained with picrosirius red to highlight interstitial collagen [26].

Control samples: rat tail samples and skeletal muscle fibres

As controls, rat tail (~100% collagen) and permeabilised skeletal muscle fibres (~0% collagen) were used. Rat tail sections were dissected in relaxing solution and collagenous strands were isolated, T-clipped and stored in relax and glycerol solution at –20°C. Skeletal muscle fibers were isolated from the psoas muscle of adult male New Zealand white rabbits. Bundles were removed and permeabilized as described previously [27]. Bundles were stored for up to 8 weeks in relax and glycerol solutions at –20°C. Single muscle fibers from bundles were isolated 1–2 mm in length and T-clipped as previously described [28].

Experimental microscope set-up and imaging acquisition setting

All samples were mounted in relaxing solution between hooks on a custom-made set-up optimized for fitting the microscope stage. Two-photon excitation and SHG imaging was performed using a Leica TCS SP5 upright laser scanning system (Leica Microsystems), coupled to a titanium:sapphire laser (Spectraphysics Mai Tai 690–1020 nm, 90 MHz; Spectra-Physics, Santa Clara, CA). All imaging was performed with an excitation wavelength of 900 nm (except for the spectra collection) with an average power of ~10–12 mW (except for the power calibration measurements) at the specimen using a long working distance water immersion objective 25 \times 0.9NA. Typical acquisition parameters are the following: 512 \times 512 pixels, zoom 2.5, pixel size 0.53 \times 0.53 μm , Kalman average of four images, pixel dwell time 18.75 μs , z-step size 0.4 μm . The SHG was collected in the backward direction by selecting the 440–460 nm range while autofluorescence light was collected in the 500–700 nm range. Typical z-stack of 100–150 μm have been acquired simultaneously collecting B_{SHG} and TPE autofluorescence. Lambda stacks for spectral analysis were collected from 390 nm to 700 nm (10 nm increments) exciting at different two-photon excitation wavelengths from 800 nm to 940 nm (20 nm increments). B_{SHG} versus excitation power were performed by varying the neutral filter at the laser output to increase the excitation power: power was measured after the objective (directly onto the samples) with a power meter (Thorlabs), ranging from 10 mW up to 70 mW. Forward vs Backward SHG measurements were performed by collecting 3D sectioning at different NaCl concentrations (0, 25 mM, 50 mM, 100 mM, 200 mM) compared to relaxing solution. Polarization

measurements were performed by rotating the stage in 10-degree increments. Intensity and volumetric analysis are performed on SHG and autofluorescence stacks using a custom-designed macro within the Java-based program ImageJ (<http://rsb.info.nih.gov/ij/>).

Statistical analysis

In this study 16 animals (8MI and 8AMC) were used. From each animal 2–3 trabecular preparations were excised for imaging analysis. For each trabecula, four z-stacks (each nearly 100 μm depth) were collected in different areas (248 μm \times 248 μm) of the sample in order to control for inter sample variability. Both the intensity and the volume analysis are presented as mean and standard deviation.

Results

Collected light characterisation

Histological sections of left ventricular tissues stained with Picrosirius Red (PR) are used to determine the biological origin of the SHG and autofluorescence signal collection. As shown in Fig. 1, (a and b from myocardial infarction tissues; c from age-matched control) SHG light discriminates collagen I with a better signal to noise ratio than PR, while autofluorescence highlights elastin and other components in the myocytes. It is worth underlining that Picrosirius Red stains both collagen type I and type III, without discriminating between the two and it is affected by unspecific binding; SHG is mainly due to type I as type III signal is probably too weak to be detected in the light collection arrangement used here. Overall these images show qualitative similarity between the two methods, with some mismatches. Nonetheless the SHG images show higher contrast and better specificity to detect collagen than PR. To demonstrate the physical origin of the signal, emission spectra are collected at different excitation wavelengths to distinguish B_{SHG} from autofluorescence. As shown in Fig. 1d, B_{SHG} peaks at exactly half the excitation wavelength, as expected from theory, correspondingly shifting with it, while autofluorescence spectra neither change shape or shift, showing a weaker intensity in a much broader λ -range. This spectral analysis represents the identity card of the collected light allowing for optimisation of excitation-emission settings. In experiments shown here, 900 nm excitation is a convenient compromise between B_{SHG} intensity, low autofluorescence (but still useful to outline the sample volume), penetration depth and Ti-sapphire laser performance.

Calibration on rat tail samples and permeabilised skeletal muscle fibres:

1. **Excluding myosin-SHG.** In biological tissue, SHG has been shown to arise from collagen, microtubules as well as myosin [6,13,29,30]. In order to assess changes in collagen deposits induced by cardiac disease, measurements rely on a signal arising solely from collagen, collagen-SHG. Determination of the origin of SHG was carried out by varying the excitation power of laser illumination on skeletal muscle fibres (Fig. 2 a, c, e, g) and cardiac tissue (Fig. 2 b, d, f, h). The B_{SHG} signal generated in Type II skeletal muscle fibres arises only from myosin while the one generated in cardiac tissues arises from both myosin and collagen: in this case, despite both collagen-SHG and myosin-SHG generate light at the same wavelength, the different localization within the muscle tissue allows for discriminating the two signals. In Fig. 2i, it can be seen that B_{SHG} generation by myosin requires very much higher laser intensity at 900 nm than collagen. Other excitation wave-

lengths were tested at increasing powers inducing a similar response (data not shown). In the power range 10 to 20 mW, the myosin-SHG signal can be ignored as it contributes to less than 5% of the total with a good signal to noise ratio for the collagen-SHG collection. All the measurements on infarcted and healthy cardiac tissues were performed at 10–12 mW, thus also limiting the induction of photodamage.

2. **Maximising Backward Collection.** While fluorescence is isotropic and hence emitted in all directions, SHG is anisotropic because of phase matching considerations and hence highly directional [31]. It is primarily forward directed, but imperfect phase matching causes SHG emission from tissues to have a distribution of components emitted forward (F) and backward (B) [14,32]. As Williams et al. (2005) showed in addressing the origin of SHG from collagen [13], the directionality is highly dependent on the ionic strength of the solution in which the sample is analyzed. In particular they showed that at a physiological level of extracellular NaCl the F/B ratio decreases. We repeated this type of experiment by acquiring only B_{SHG} on rat tail fibrils at different NaCl concentrations in comparison with the relaxing solution used to image fresh cardiac tissues, at an ionic strength comparable to physiological saline concentrations (see materials for exact composition). Fig. 3 clearly shows the increase of B_{SHG} with increasing NaCl concentration, reaching saturation above 50 mM NaCl; measurements performed in relaxing solution were also at the plateau, demonstrating that in our experimental conditions, we maximize the B_{SHG} collection. It is worth noting however that the B_{SHG} we refer to, collected in the epi-mode, is partly due to true backward-SHG and partly due to back-scattered forward-SHG. This means that even though the truly backward SHG light intensity is usually quite small, with the contribution from the back-scatter a measurable SHG signal is obtained in tissue. Optimizing the ionic strength of the solution further maximizes the signal collection.
3. **Polarization effect.** SHG intensity is dependent on the angle between the collagen fibrils and the polarization of incident light [33]. Calibration measurements were performed on rat tail samples to evaluate the dependence on polarization angle by rotating the microscope stage in 10 degree steps (see Figure S1). The SHG intensity variation measured at different polarization directions is in agreement with the literature [29,34]. We experimentally observed a small intensity modulation (nearly 6%) compared to previously published values [35,36] because the polarization status at the focus is elliptical and the tail samples contain fibrils with different orientations, thus flattening the response. It was necessary to determine the role of polarization in our instrument to ensure that in our experimental conditions the polarization direction didn't affect the evaluation of the increase in B_{SHG} seen in MI samples compared to AMC. As an added precaution, the infarcted or healthy samples were imaged in the same orientation under the microscope. The experimental observation suggests that collagen fibres in both healthy and in diseased samples are mainly parallel to the main muscle axis. It is worth noting that increased fibrosis in diseased samples could lead to the appearance of collagen fibres which are not parallel to the main muscle axis, in the worse case perpendicular to it. In this case the B_{SHG} intensity evaluated would be underestimated by 6%. The use of circularly-polarized light would eliminate polarization-induced intensity differences.
4. **Detection Range.** Measurements to determine the B_{SHG} detection range were performed on rat tail samples, skeletal

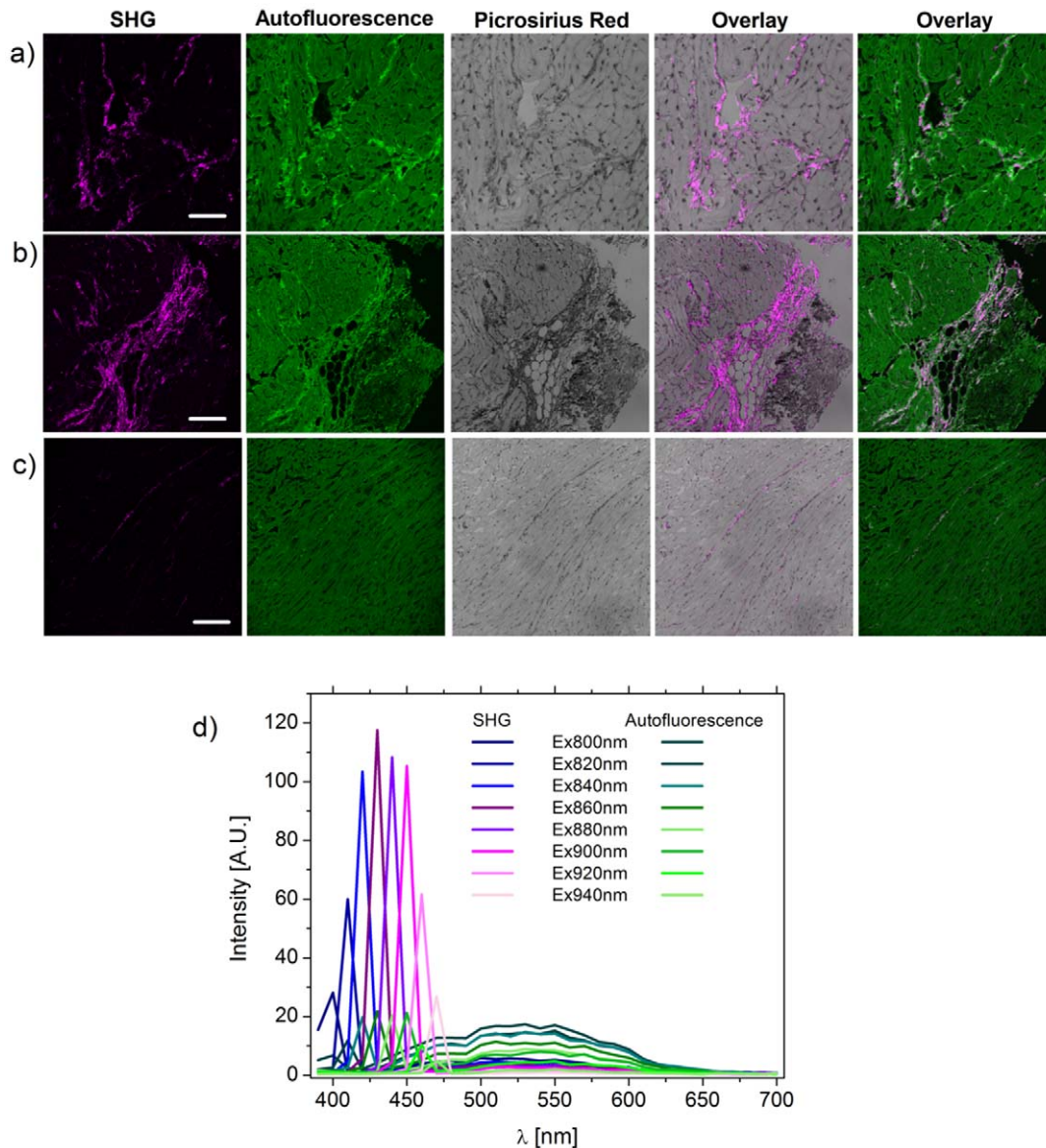


Figure 1. B_{SHG} and autofluorescence characterisation. Standard histology sections are stained with picosirius red to highlight collagen in tissues from myocardial infarction rat model (a and b), from age-match control in c, showing the better signal to noise ratio for SHG light in discriminating collagen. In d, the spectral characterization is presented to demonstrate that the collected signals are SHG (magenta) by observing the shift in peak intensity with that of the excitation wavelength and autofluorescence (green). Scale bar 50 μm in a, 100 μm in b and c. doi:10.1371/journal.pone.0056136.g001

muscle fibres and cardiac trabeculae. We used rat tail samples as positive control because they are mainly composed of collagen type I, and single permeabilised skeletal muscle fibres as negative control because the permeabilisation process removes the outer membrane and the thin collagen sheath surrounding it. Fig. 4 shows the intensity of B_{SHG} collected for rat tail (black), three trabeculae (dark grey) and two skeletal fibres (light grey), normalized to the tail B_{SHG} intensity. The rat tail B_{SHG} response represents indeed the upper bound of detection; permeabilised skeletal fibres show little collagen and define the lower limit of detection (1–2% of rat tail signal); cardiac trabeculae from healthy hearts show a small but detectable intensity (5–6%) of B_{SHG} with respect to the tail, thus ensuring a maximal range (95%) allowance for the increased fibrosis expected in samples from infarcted hearts.

5. Penetration Depth. SHG intensity is limited by penetration depth. Depth attenuation is ruled by bulk optical properties: absorption coefficient, scattering, refractive index, etc. Experimentally the excitation light at the range of wavelengths used here (800–950 nm) is limited to 200–300 μm depth, depending on the tissue turbidity and scatterers distribution. The backward light collected (B_{SHG} convolved with scattering) rapidly decays within the first 100 μm as shown in Fig. 4 for rat tail segments. All the measurements were performed on trabecular preparations (the same muscle tissue) of similar thickness (in the range of 100–120 μm), so that similar scattering and attenuation effects are expected for the test and control trabeculae. In order to improve the penetration depth, clearing agents [32,37] as well as adaptive optics [38,39] could be employed. A 50% glycerol treatment has been already

used in the sample preparation, allowing for a maximum penetration depth of nearly 100 μm , as shown in Fig. 4 and Fig. 5. Future measurements of the depth-dependent SHG directionality and attenuation responses in conjunction with simulations based on the bulk optical parameters [17] could refine our quantitative analysis.

Quantifying disease by Intensity Analysis

To quantitatively analyze the increase in fibrosis, optical sectioning measurements were performed on non-infarcted trabeculae extracted from rats sacrificed 20 weeks following myocardial infarction (8MI samples) in comparison with age-match controls (8AMC samples), by simultaneously acquiring B_{SHG} arising from collagen and autofluorescence from elastin and other myocyte proteins. The autofluorescence image is used to define the edges of the sample, by thresholding the autofluorescence intensity as depicted in Fig. 5a. The same region of interest is then applied to the B_{SHG} image (Fig. 5b) in order to evaluate the intensity in that area. This process is repeated through all the images acquired in the z-stack in order to measure the B_{SHG} signal throughout the thickness of the sample analyzed. In Fig. 5c the B_{SHG} intensity (measured as described above) of 3 MI samples is presented in comparison with 2 AMC samples as an example. Clearly an increased B_{SHG} intensity can be observed due to the increased fibrosis. But even more interestingly, a different spatial distribution through the sample thickness can be outlined. Control samples show a more superficial presence of collagen (the first 10 μm), while in the MI samples the B_{SHG} intensity increases also in central layers (see Video S1 and S2 for the entire z-stack and 3D rendering examples). To quantitatively evaluate the B_{SHG} intensity increase in the MI samples with respect to the controls the integral over 10 μm steps is performed and the mean and standard deviation is evaluated for the two groups. Fig. 5d shows the

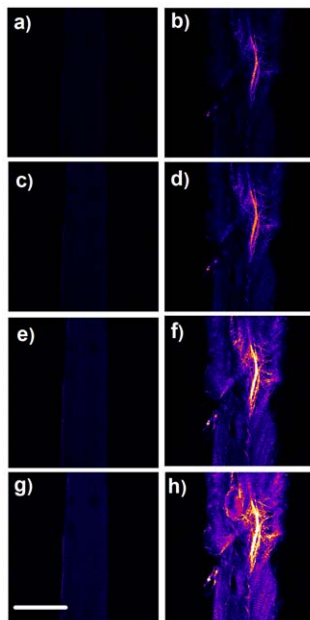


Figure 2. Myosin- B_{SHG} detection. Skeletal fibres (a, c, e, g, circle symbols in the graph) and cardiac trabeculae (b, d, f, h, squared symbols in the graph) imaged at increasing excitation power ranging from 10 mW up to 70 mW at 900 nm. In i), filled squared symbols are related to collagen- B_{SHG} , while open squared symbols are related to myosin- B_{SHG} , obtained from analyzing region of interest showing only collagen fibrosis or sarcomeric proteins respectively, as these are well spatially separated. By utilizing low power (10–20 mW) myosin- B_{SHG} can be neglected, thus ensuring the collection of only collagen- B_{SHG} . Scale bar 100 μm . doi:10.1371/journal.pone.0056136.g002

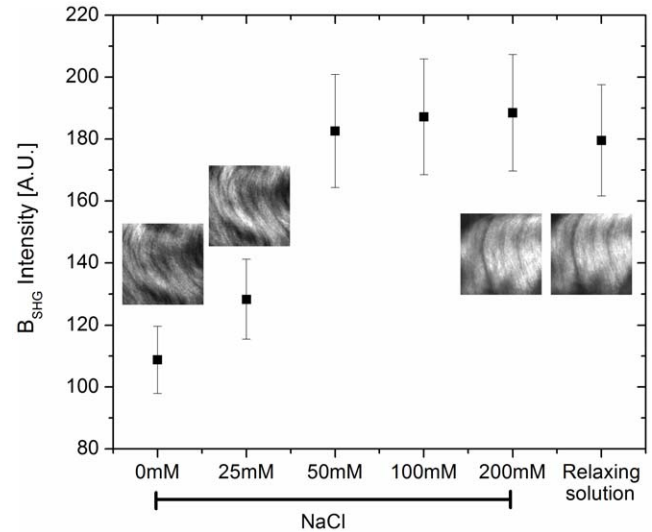
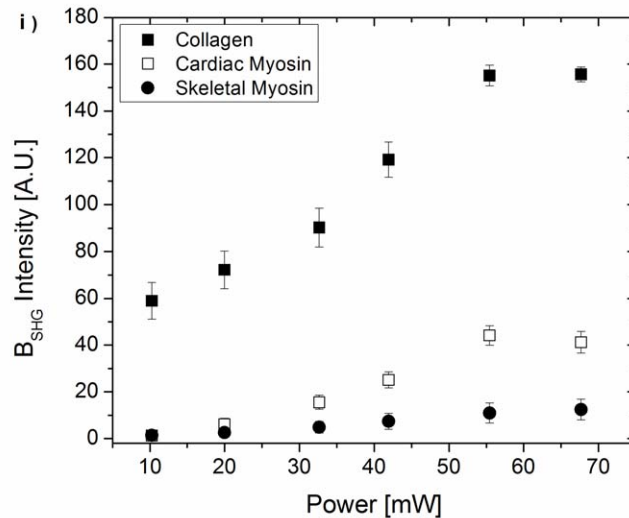


Figure 3. B_{SHG} dependence on ionic strength. B_{SHG} from rat tail samples has been collected at different NaCl concentrations compared to relaxing solution. From 50 mM NaCl the B_{SHG} reaches a plateau. Measurements performed in relaxing solution fall in the same range of intensity ensuring that in the present experimental conditions we maximize the backward light collection. Images above symbols are representative for that concentration. doi:10.1371/journal.pone.0056136.g003

average intensity increase for each 10 μm step in the z-direction. All the controls analyzed showed a very similar distribution throughout all the thickness, while the MI samples show differences in collagen distribution along the z axis, reflected in the large standard deviation of the average intensity increase. On average, in the first superficial layers (20–30 μm) MI samples



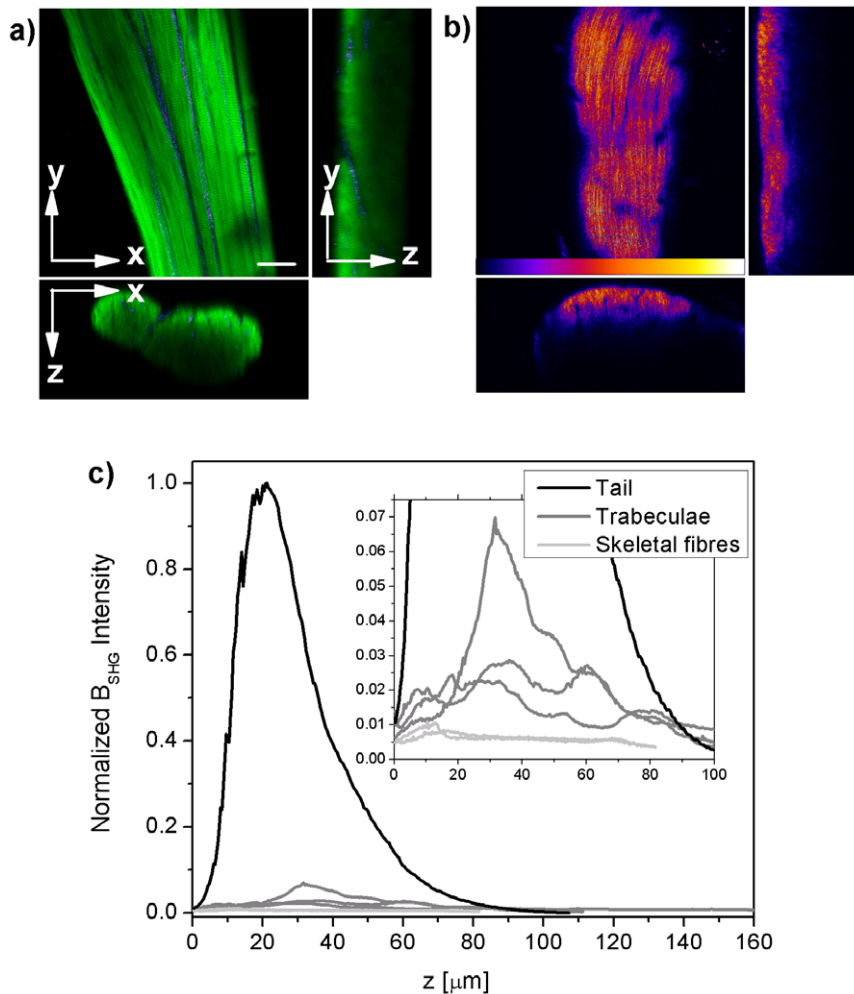


Figure 4. Upper and lower B_{SHG} detection range. Representative 3D optical sections (xy and orthogonal view xz, yz) of a trabecula in a) and a rat tail in b); green autofluorescence, fire color scale B_{SHG} . Scale bar, 25 μm . In c) B_{SHG} intensity versus sample depth is presented for rat tail samples (black), cardiac trabeculae (dark grey) and permeabilised skeletal fibres (light grey). Intensity profiles have been normalized to the rat tail samples as they represent the upper bound of B_{SHG} detection. On the contrary permeabilised skeletal fibres show virtually no B_{SHG} (2%) thus representing the lower bound of detection. Healthy cardiac samples show a low but measurable B_{SHG} , thus ensuring a large range of detection for possible increases in collagen content in diseased samples. doi:10.1371/journal.pone.0056136.g004

report nearly a 3-fold increase in B_{SHG} intensity (note that AMC samples show the presence of superficial collagen). More interestingly, at higher depth the B_{SHG} intensity ratio (MI/AMC) increases up to 6-fold, demonstrating the appearance of new collagen, not present in the AMC samples.

Quantifying disease by Volume Analysis

Finally we used autofluorescence and B_{SHG} to assess the volume of collagen in our samples. The autofluorescence image (Fig. 6a) is used to specify the selected tissue area in each optical slice (number of pixels). The B_{SHG} image is thresholded to count the number of pixels showing a B_{SHG} signal above background as illustrated in Fig. 6b. Repeating this process for each layer of the z-stack, a discretized volume for the sample and collagen is obtained from the autofluorescence and B_{SHG} images respectively. Fig. 6c shows the number of pixels evaluated for each z-layer (black and red lines from autofluorescence; orange and grey lines from B_{SHG}): these data are normalized so that the area under the autofluorescence-related curves is equal to unity, hence representing the total volume of that sample, and the B_{SHG} -related curves representing

the percentage of collagen in that volume. Red and orange curves refer to MI samples; black and grey lines represent AMC samples. By integrating orange and grey curves the fraction of collagen present in that volume is then calculated. Fig. 6d shows the average collagen presence evaluated for the two groups MI and AMC (mean and st.dev from 8 animals each group). The MI samples show a 5-fold increase in volume occupied by collagen with respect to the AMC.

Discussion

The aim of the present study is to measure and accurately quantify collagen accumulation, a feature of fibrosis induced by cardiac disease. In particular we study the example of cardiac disease in a rat model of chronic post myocardial infarction heart failure. Routine histology and immunohistochemistry are useful tools to identify the levels of increased fibrosis induced by cardiac disease, but they are inadequate to quantify the total collagen presence and the induced structural changes in fresh, untreated tissues. By contrast non-linear optical techniques as those used

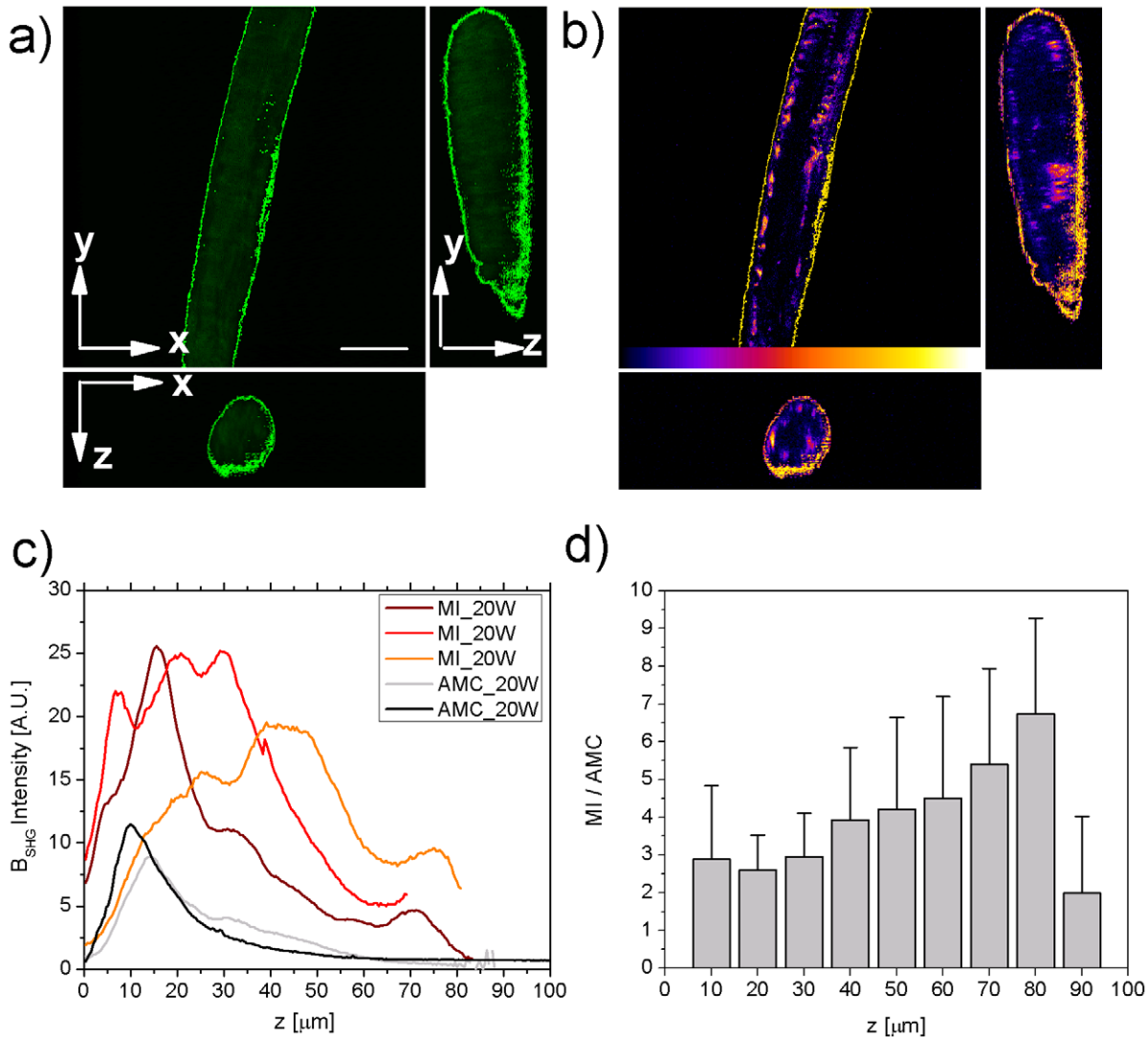


Figure 5. Intensity Analysis. 3D (shown as xy view and orthogonal views xz, yz) autofluorescence a) and B_{SHG} b) from a MI sample. The region of interest selected by thresholding the autofluorescence to define the sample edges is highlighted in green in a); the very same region is applied to the B_{SHG} images, highlighted in yellow in b); c) intensity profile along the thickness of the sample, MI (dark red, red, orange), AMC black and grey; d) Average intensity increase (MI/AMC) obtained by integrating B_{SHG} intensity over 10 μm z-steps. doi:10.1371/journal.pone.0056136.g005

here present an attractive alternative to evaluate these morphological adaptations to disease *in vivo*. In particular, to quantitatively evaluate the collagen presence in the myocardium, a careful calibration of the acquisition settings is presented by performing measurements on rat tail samples and permeabilised skeletal muscle fibres as controls. In particular we show how to specifically separate SHG arising from collagen and SHG arising from myosin, by utilizing powers ranging from 10 to 20 mW (see Fig. 2i); we maximize the backward collection by controlling the solution ionic strength (see Fig. 3); and we minimize the effect of laser polarization by imaging rat samples in the same orientation. These calibrations are essential to quantitatively evaluate collagen presence within the myocardium. It's worth noting that by acquiring only the backward signal we are limited in quantifying the total collagen presence in absolute terms, particularly we may underestimate the collagen presence as there might be collagen fibrils whose backward signal is too low to be detected. This limit can be overcome by embedding within the tissue fluorescent beads

which can be used as intensity normalization standards as fluorescence is isotropic thus not influenced by directionality. Still the method presented here provides comparative measurements and careful calibration of the system as shown here can yield quantitative results.

In the rat heart failure model, a 5-fold increase in collagen fibrosis is measured in the remote viable myocardium 20 weeks after infarction. Our results show a marked change in collagen distribution (see Fig. 5–6 and Video S1): AMC samples present, as expected, a thin extracellular superficial collagen sheath surrounding the left ventricular portion analyzed, while in the MI samples, collagen appears in between bundles of myocytes disrupting their precise networking organization. Specifically, elevated interstitial fibrosis, as shown here, may reduce tissue compliance and impair both contraction and relaxation [4]. Fibrosis also can disrupt conduction pathways and the patchy distribution may result in electrical heterogeneities which may be proarrhythmic [2]. These results confirm that an increase in collagen in tissue from the non-

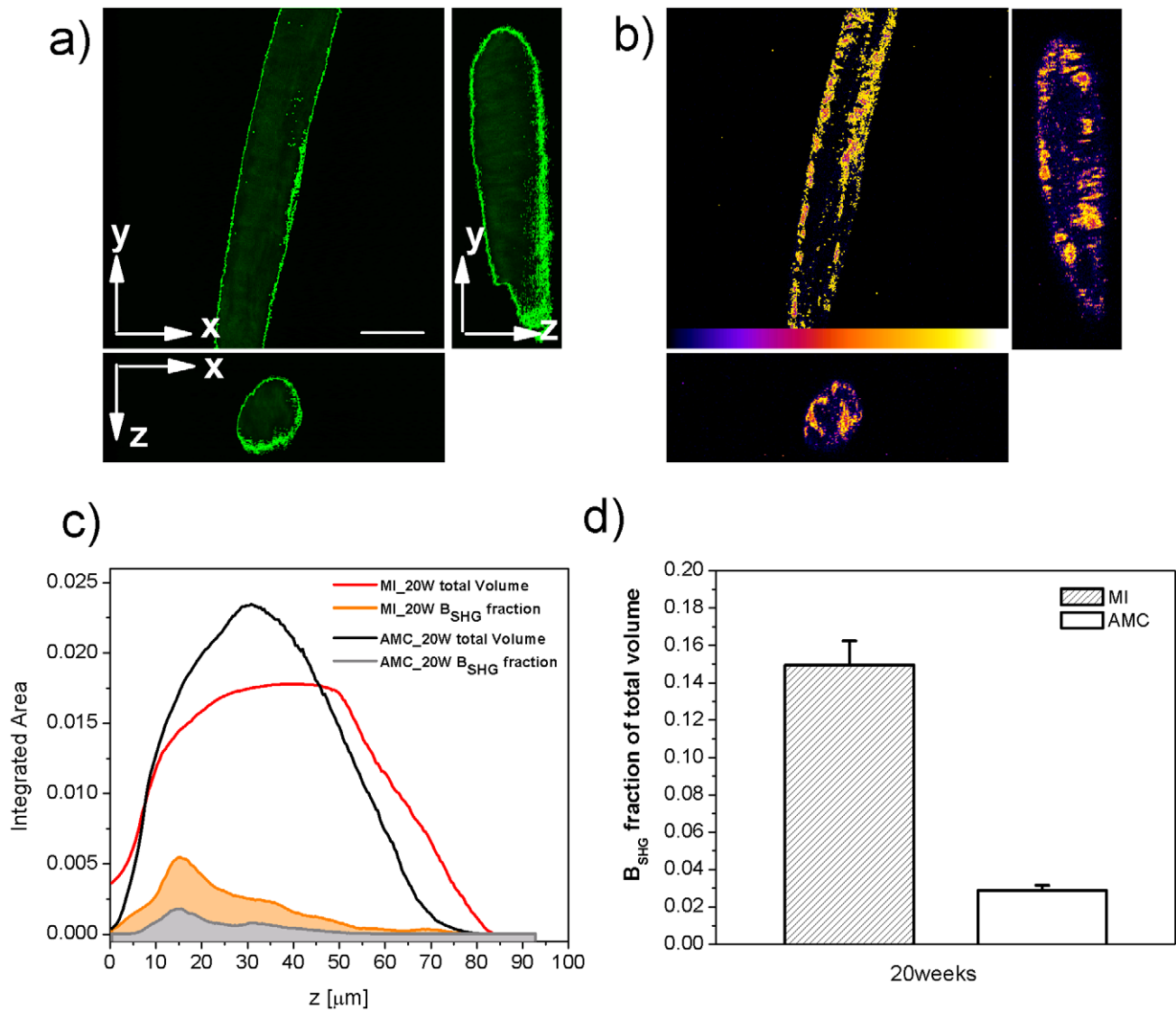


Figure 6. Volume Analysis. 3D (shown as xy view and orthogonal views xz, yz) autofluorescence a) and B_{SHG} b) from a MI sample. The region of interest selected by thresholding the autofluorescence to define the total volume of the sample is highlighted in green in a); the region of interest selected by thresholding the B_{SHG} to define the volume occupied by collagen is highlighted in yellow in b); c) the discretized area vs depth is plotted, black and red is from autofluorescence (AMC and MI samples respectively) grey and orange from B_{SHG} (AMC and MI sample respectively); the curves have been normalized so that the integral over black and red is 1, therefore representing the total volume, and over grey and orange is the fraction of volume occupied by collagen; d) average collagen presence evaluated for MI (n=8) compared to AMC (n=8) animals.
doi:10.1371/journal.pone.0056136.g006

infarcted portion of rat hearts following myocardial infarction is an important part of the adverse cardiac remodelling that occurs in this disease. Although it is known that increased fibrosis is one of the reasons for the progressive decline in cardiac function post myocardial infarction, this novel technique allows assessment of this process quantitatively, in 3-D and with excellent spatial resolution. Besides the overall image quality improvement obtained thanks to the high specificity of the B_{SHG} light arising from collagen, which gives a better signal to noise ratio than routine histology methods, the 3D information gained by analyzing fresh, untreated tissue will be extremely useful to study myocardium adaptation to collagen increase. It is worth noting that all the measurements were carried out on trabecular preparations. Trabeculae should be representative of the LV wall's full thickness, but similar measurements in other regions of the myocardium should be performed. We used trabeculae as

these represent the usual standards for mechanical measurements in order to couple the structural information obtained here with methods to probe the mechanical properties of the exact same samples. This combined approach will be unique in giving an insight into the structure-function relationship of the heart. It is particularly important to be able to visualize and quantify myocardial fibrosis, coupled to the mechanical response, in the burgeoning field of anti-fibrotic myocardial therapeutics [40,41] where such quantification will be invaluable in the assessment of efficacy of the agents used.

Longer term we can foresee applicability of this technique beyond biomedical research and into clinical practice. The application of such a technique in conjunction with imaging endoscopes [42,43] could open the door towards targeted local or systemic therapy for collagen deposition in heart failure.

Supporting Information

Figure S1 The dependence of B_{SHG} intensity on polarization has been characterized on rat tail samples by rotating the microscope stage in 10 degree steps. The x-axis represents the angle between the main axis of the collagen fibre and the major axis of the laser polarization at the focus. A small intensity modulation (nearly 6%) is observed because the polarization status at the focus is elliptical and the tail samples presented fibrils at different orientation, thus flattening the response. However, this result ensures that in our experimental conditions, the polarization direction doesn't affect the evaluation of the increase in B_{SHG} seen in MI samples compared to AMC. (TIF)

Video S1 Optical sectioning example of a MI sample showing B_{SHG} in fire pseudo scale colour and autofluorescence in green. (AVI)

Video S2 3D rendering of the MI sample in movie1 showing B_{SHG} in fire pseudo scale colour and autofluorescence in green.

(AVI)

Acknowledgments

We acknowledge the FILM facility (Facility for Imaging by Light Microscopy) of Imperial College, and L. Lawrence for the histology sections. We are indebted to Professor W.R. Zipfel and Professor Mark Neil for the useful discussions.

Author Contributions

Conceived and designed the experiments: VC CT MAF. Performed the experiments: VC CT MBS. Analyzed the data: VC. Contributed reagents/materials/analysis tools: CT MBS ARL KM. Wrote the paper: VC CT MBS ARL KM MAF.

References

- Burlew BS, Weber KT (2000) Connective tissue and the heart. *Functional significance and regulatory mechanisms.* *Cardiol Clin* 18: 435–442.
- Khan R, & Sheppard R (2006) Fibrosis in heart disease: understanding the role of transforming growth factor- β 1 in cardiomyopathy, valvular disease and arrhythmia. *Immunology* 118: 10–24.
- Chen J, Koo Lee S, Abd-Elgaliel RW, Liang L, Galende E, et al. (2001) Assessment of Cardiovascular Fibrosis Using Novel Fluorescent Probes. *PlosOne* 6(4): e19097.
- Klein G, Schaefer A, Hilfiker-Kleiner D, Oppermann D, Shukla P, et al. (2005) Increased Collagen Deposition and Diastolic Dysfunction but Preserved Myocardial Hypertrophy After Pressure Overload in Mice Lacking PKC ϵ . *Circ Res* 96: 748–755.
- Schenke-Layland K, Stock AU, Nsair A, Xie J, Angelis E, et al. (2009) Cardiomyopathy is associated with structural remodelling of heart valve extracellular matrix. *Eur Heart J* 30: 2254–2265.
- Chen X, Nadiarynk O, Plotnikov S, Campagnola PJ (2012) Second harmonic generation microscopy for quantitative analysis of collagen fibrillar structure. *Nat Protoc* 7(4): 654–669.
- Zipfel RW, Williams RM, Webb WW (2003) Nonlinear magic: multiphoton microscopy in the biosciences. *Nat Biotech* 21 (11): 1369–1377.
- He GS, Liu SH (1999) *Physics of nonlinear optics.* World Scientific Publishing Co., Singapore.
- Oheim M, Michael DJ, Geisbauer M, Madsen D, Chow RH (2006) Principles of two-photon excitation fluorescence microscopy and other nonlinear imaging approaches. *Advanced Drug Delivery Reviews* 58: 788–808.
- Diaspro A, Caorsi V, Bianchini P, Chirico G, Usai C (2006) *Multiphoton Microscopy in: Akay M, ed. Wiley Encyclopedia of Biomedical Engineering.* John Wiley & Sons; Hoboken, New Jersey.
- Campagnola PJ, Loew LM (2003) Second-harmonic imaging microscopy for visualizing biomolecular arrays in cells, tissues and organisms. *Nat Biotechnol* 21: 1356–1360.
- Campagnola PJ, Wei MD, Lewis A, Loew LM (1999) High-Resolution Nonlinear Optical Imaging of Live Cells by Second Harmonic Generation. *Biophys J* 77(6): 3341–9.
- Williams RM, Zipfel WR, Webb WW (2005) Interpreting Second-Harmonic Generation Images of Collagen I Fibrils. *Biophys J* 88: 1377–1386.
- LaComb R, Nadiarynk O, Townsend SS, Campagnola PJ (2008) Phase Matching considerations in Second Harmonic Generation from tissues: Effects on emission directionality, conversion efficiency and observed morphology. *Opt Commun* 281(7): 1823–1832.
- Han M, Giese G, Bille JF (2005) Second harmonic generation imaging of collagen fibrils in cornea and sclera. *Opt Express* 13(15): 5791–5797.
- Sun W, Chang S, Tai DCS, Tan N, Xiao G, et al. (2008) Nonlinear optical microscopy: use of second harmonic generation and two-photon microscopy for automated quantitative liver fibrosis studies. *J Biomed Opt* 13(6): 064010.
- LaComb R, Nadiarynk O, Campagnola PJ (2008) Quantitative Second Harmonic Generation Imaging of the Diseased State Osteogenesis Imperfecta: Experiment and Simulation. *Biophys J* 94: 4504–4514.
- Schenke-Layland K, Riemann I, Stock UA, Konig K (2005) Imaging of cardiovascular structures using near-infrared femtosecond multiphoton laser scanning microscopy. *J Biomed Opt* 10(2): 024017.
- Tsai MR, Chiu YW, Lo MT, Sun CK (2010) Second-harmonic generation imaging of collagen fibers in myocardium for atrial fibrillation diagnosis. *J Biomed Opt* 15(2): 026002.
- Wallenburg MA, Wu J, Li R, Vitkin IA (2011) Two-photon microscopy of healthy, infarcted and stem-cell treated regenerating heart. *J Biophotonics* 4(5): 297–304.
- Lyon AR, MacLeod KT, Zhang Y, Garcia E, Kanda GK, et al. (2009) Loss of T-tubules and other changes to surface topography in ventricular myocytes from failing human and rat heart. *Prot Natl Acad Sci* 106(16): 6854–6859.
- Francis GS, Chu C (1995) Post-infarction myocardial remodelling: why does it happen? *Eur Heart J* 16 (Supplement N): 31–36.
- Cittadini A, Monti MG, Isgaard J, Casaburi C, Stromer H, et al. (2003) Aldosterone receptor blockade improves left ventricular remodeling and increases ventricular fibrillation threshold in experimental heart failure. *Cardiovasc Res* 58(3): 555–64.
- See F, Kompa A, Martin J, Lewis DA, Krum H (2005) Fibrosis as a therapeutic target post-myocardial infarction. *Curr Pharm Des* 11(4): 477–87.
- Sato M, O'Gara P, Harding SE, Fuller SJ (2005) Enhancement of adenoviral gene transfer to adult rat cardiomyocytes in vivo by immobilization and ultrasound treatment of the heart. *Gene Ther* 12: 936–941.
- Kiernan JA (1999) *Histological and histochemical methods: Theory and practice, Ed. 3.* Butterworth Heinemann, Oxford, UK.
- Thirlwell H, Corrie JE, Ferenczi MA (1994) Kinetics of relaxation from rigor of permeabilized fast-twitch skeletal fibers from the rabbit using a novel caged ATP and apyrase. *Biophys J* 67: 2436–2447.
- Goldman YE, Simmons RM (1994) Control of sarcomere length in skinned muscle fibres of *Rana temporaria* during mechanical transients. *J Physiol* 350: 497–518.
- Plotnikov SG, Millard AC, Campagnola PJ, Mohler WA (2006) Characterization of the Myosin-Based Source for Second-Harmonic Generation from Muscle Sarcomeres. *Biophys J* 90: 693–703.
- Psilodimitrakopoulos S, Petegnief V, Soria G, Amat-Roldan I, Artigas D, et al. (2009) Estimation of the effective orientation of the SHG source in primary cortical neurons. *Opt Express* 17(16): 14418–14425.
- Zipfel WR, Williams RM, Christie R, Nikitin AY, Hyman BT, et al. (2003) Live tissue intrinsic emission microscopy using multiphoton-excited native fluorescence and second harmonic generation. *Prot Natl Acad Sci* 100(12): 7075–7080.
- Campagnola PJ (2012) Second Harmonic Generation Imaging Microscopy: Applications to Diseases Diagnostics. *Anal Chem* 83(9): 3224–3231.
- Gusachenko I, Tran V, Housen YG, Allain J, Schanne-Klein M (2012) Polarization-Resolved Second-Harmonic Generation in Tendon upon Mechanical Stretching. *Biophys J* 102: 2220–2229.
- Su P, Chen W, Chen Y, Dong C (2011) Determination of Collagen Nanostructure from Second-Order Susceptibility Tensor Analysis. *Biophys J* 100: 2053–2062.
- Ambekar R, Lau T, Walsh M, Bhargava R, Toussaint KC (2012) Quantifying collagen structure in breast biopsies using second-harmonic generation imaging. *Biomed Optic Express* 3(9): 2021–2035.
- Latour G, Gusachenko I, Kowalczyk L, Lamarre I, Schanne-Klein M (2012) In vivo structural imaging of the cornea by polarization-resolved second harmonic microscopy. *Biomed Optic Express* 3(1): 1–15.
- LaComb R, Nadiarynk O, Carey S, Campagnola PJ (2008) Quantitative second harmonic generation imaging and modeling of the optical clearing mechanism in striated muscle and tendon. *J Biomed Opt* 13(2): 021109.
- Thayil A, Watanabe T, Jesacher A, Wilson T, Srinivas S, et al. (2011) Long-term imaging of mouse embryos using adaptive harmonic generation microscopy. *J Biomed Opt* 16(4): 046018.
- Booth M (2007) Adaptive optics in microscopy. *Phil Trans R Soc A* 365: 2829–2843.
- Zhang Y, Edgley AJ, Cox AJ, Powell AK, Wang B, et al. (2012) FT011, a new anti-fibrotic drug, attenuates fibrosis and chronic heart failure in experimental diabetic cardiomyopathy. *Eur J Heart Fail* 14(5):549–62.

41. Edgley AJ, Krum H, Kelly DJ (2012) Targeting fibrosis for the treatment of heart failure: a role for transforming growth factor- β . *Cardiovasc Ther* 30(1): e30–40.
42. Rivera DR, Brown CM, Ouzounov DG, Pavlova I, Kobat D, et al. (2011) Compact and flexible raster scanning multiphoton endoscope capable of imaging unstained tissue. *Proc Natl Acad Sci* 108(43): 17598–17603.
43. Wu Y, Leng Y, Xi J, Li X (2009) Scanning all-fiber-optic endomicroscopy system for 3D nonlinear optical imaging of biological tissues. *Opt Express* 17(10): 7907–7915.